Spin-Injection Spectroscopy of a Spin-Orbit Coupled Fermi Gas

Lawrence W. Cheuk, Ariel T. Sommer, Zoran Hadzibabic, Tarik Yefsah, Waseem S. Bakr, and Martin W. Zwierlein

Phys. Rev. Lett. **109**, 095302 — Published 27 August 2012

DOI: 10.1103/PhysRevLett.109.095302

Spin-Injection Spectroscopy of a Spin-Orbit Coupled Fermi Gas

Lawrence W. Cheuk,[1] Ariel T. Sommer,[1] Zoran Hadzibabic,[1,2]
Tarik Yefsah,[1] Waseem S. Bakr,[1] and Martin W. Zwierlein[1]

[1]*Department of Physics, MIT-Harvard Center for Ultracold Atoms, and Research Laboratory of Electronics, MIT, Cambridge, Massachusetts 02139, USA*
[2]*Cavendish Laboratory, University of Cambridge, J. J. Thomson Avenue, Cambridge CB3 0HE, United Kingdom*

The coupling of the spin of electrons to their motional state lies at the heart of recently discovered topological phases of matter. Here we create and detect spin-orbit coupling in an atomic Fermi gas, a highly controllable form of quantum degenerate matter. We directly reveal the spin-orbit gap via spin-injection spectroscopy, which characterizes the energy-momentum dispersion and spin composition of the quantum states. For energies within the spin-orbit gap, the system acts as a spin diode. We also create a spin-orbit coupled lattice and probe its spinful band structure, which features additional spin gaps and a fully gapped spectrum. In the presence of s-wave interactions, such systems should display induced p-wave pairing, topological superfluidity, and Majorana edge states.

Spin-orbit coupling is responsible for a variety of phenomena, from the fine structure of atomic spectra to the spin Hall effect, topological edge states, and in the presence of interactions, the predicted phenomenon of topological superconductivity [1, 2]. In electronic systems, spin-orbit coupling arises from the relativistic transformation of electric fields into magnetic fields in a moving reference frame. In the reference frame of an electron moving with wavevector $\mathbf{k}$ in an electric field, the motional magnetic field couples to the electron spin through the magnetic dipole interaction. In a two-dimensional semiconductor heterostructure, the electric field can arise from structure or bulk inversion asymmetry [3], leading to magnetic fields of the form $\mathbf{B}^{(R)} = \alpha(-k_y, k_x, 0)$ or $\mathbf{B}^{(D)} = \beta(k_y, k_x, 0)$ respectively known as the Rashba [4] and Dresselhaus [5] contributions. Including a possible momentum-independent Zeeman field $\mathbf{B}^{(Z)} = (0, B_y^{(Z)}, B_z^{(Z)})$, the Hamiltonian of the electron takes the form:

$$\mathcal{H} = \frac{\hbar^2 k^2}{2m} - \frac{g\mu_B}{\hbar}\mathbf{S}\cdot(\mathbf{B}^{(D)} + \mathbf{B}^{(R)} + \mathbf{B}^{(Z)}), \qquad (1)$$

where g is the electron g-factor, μ_B is the Bohr magneton and $\mathbf{S}$ is the electron spin.

The energy-momentum dispersion and the associated spin texture of the Hamiltonian in Eq. (1) are shown in Fig. 1(a) for $B_y^{(Z)} = 0$ and $\alpha = \beta$. In the absence of a perpendicular Zeeman field $B_z^{(Z)}$, the spectrum consists of the parabolic free particle dispersions for the two spin states that are shifted relative to each other in k-space owing to the spin-orbit interaction. For a non-zero field $B_z^{(Z)}$, a gap opens in the spectrum. This gap, known as the spin-orbit gap, has been recently observed in one-dimensional quantum wires [6, 7]. The two energy bands are spinful in the sense that the spin of an atom is locked to its momentum.

In this work, we engineer the Hamiltonian in Eq. (1) with equal Rashba and Dresselhaus strengths in an optically trapped, degenerate gas of fermionic lithium atoms via Raman dressing of atomic hyperfine states [8, 9]. Raman fields have previously been used to generate spin-orbit coupling and gauge fields in pioneering work on Bose-Einstein condensates [10–12], and recently spin-orbit coupling in Fermi gases [13]. Here, we directly measure the spinful band structure of Eq. (1), as well as the rich band structure of a spin-orbit coupled lattice. For this, we introduce spin-injection spectroscopy, which is capable of completely characterizing the quantum states of spin-orbit coupled fermions, including the energy-momentum dispersion and the associated spin-texture. By tracing the evolution of quantum states in the Brillouin zone, this method can be extended to directly measure topological invariants, such as the Chern number in a two-dimensional system [1, 2, 14].

Spin-orbit coupling is generated using a pair of laser beams that connects the second and third lowest hyperfine levels in ^{6}Li, labeled $|\downarrow\rangle$ and $|\uparrow\rangle$, via a two-photon Raman transition, as shown in Fig. 1(b) and (c). The Raman process imparts momentum $\hbar Q\hat{x}$ to an atom while changing its spin from $|\downarrow\rangle$ to $|\uparrow\rangle$, and momentum $-\hbar Q\hat{x}$ while changing the spin from $|\uparrow\rangle$ to $|\downarrow\rangle$. Defining a quasi-momentum $q = k_x + \frac{Q}{2}$ for spin $|\downarrow\rangle$ and $q = k_x - \frac{Q}{2}$ for spin $|\uparrow\rangle$, one obtains the Hamiltonian of the form given in Eq. (1) [10]. In this mapping, $B_z^{(Z)} = \hbar\Omega_R/g\mu_B$, where Ω_R is the two-photon Rabi frequency, $B_y^{(Z)} = \hbar\delta/g\mu_B$, where δ is the two-photon detuning, and $\alpha = \beta = \frac{\hbar^2 Q}{2mg\mu_B}$. In addition to providing spin-orbit coupling, the Raman beams lead to spontaneous photon scattering. For our experimental setup, the spontaneous scattering rate is $\sim$ 240 times smaller than Ω_R, slow enough to permit accurate spin-injection spectroscopy (see Supplemental Material).

We sympathetically cool ^{6}Li atoms with ^{23}Na in a magnetic trap down to a temperature of $T < 0.1T_F$, where T_F is the Fermi temperature [15]. After removal of Na

atoms, the Li atoms are transferred into an optical dipole trap formed by two orthogonal 1064nm beams. To separate the atomic hyperfine levels, we apply a magnetic field of 11.6 G. At this field, the interactions between states $|\uparrow\rangle$ and $|\downarrow\rangle$ (scattering length $20a_0$) are negligible in the experiment.

When the spin-orbit gap is opened suddenly, an atom prepared in the state $|\downarrow, k_x = q - Q/2\rangle$ oscillates between $|\downarrow, k_x = q - Q/2\rangle$ and $|\uparrow, k_x = q + Q/2\rangle$ with a momentum dependent frequency $\Delta(q)/h$, where $\Delta(q)$ is the energy difference between the bands at quasimomentum q. Such Rabi oscillations correspond to Larmor precession of the pseudo-spin in the effective magnetic field $\mathbf{B}^{(\mathrm{SO})} = \mathbf{B}^{(\mathrm{D})} + \mathbf{B}^{(\mathrm{R})} + \mathbf{B}^{(Z)}$. We have observed these oscillations by starting with atoms in $|\downarrow\rangle$, pulsing on the Raman field for a variable duration τ, and imaging the atoms spin-selectively after time-of-flight expansion from the trap. Time-of-flight maps momentum to real space, allowing direct momentum resolution of the spin populations. As a function of pulse duration, we observe oscillations of the spin polarization with momentum-dependent frequencies, as shown in Fig. 1(d). Since our Fermi gas occupies a large range of momentum states with near-unity occupation, each image at a given pulse duration τ contains information for a large range of momenta q. The observation of momentum-dependent oscillations demonstrates the presence of a spin-orbit gap, and shows that the atomic systfem is coherent over many cycles. To highlight the momentum selectivity of this process, we prepare an equal mixture of atoms in states $|\uparrow\rangle$ and $|\downarrow\rangle$ and pulse on the Raman fields for a time $t = \pi/\Omega_R$ for different two-photon detunings δ. This inverts the spin for atoms with momentum q where $\Delta(q)$ is minimal and equals $\hbar\Omega_R$. The resonant momentum class depends linearly on δ due to the Doppler shift $\propto k_x Q$, as shown in Fig. 1(e).

Instead of pulsing on the Raman field and projecting the initial state into a superposition of states in the two bands, one can introduce the spin-orbit gap adiabatically with respect to band populations. This is achieved by starting with a spin-polarized Fermi gas and sweeping the two-photon detuning δ from an initial value δ_i to a final detuning δ_f. The magnitude of the initial detuning $|\delta_i|$ is much larger than the two-photon recoil energy $E_R = \hbar^2 Q^2/2m$, so that the effective Zeeman field is almost entirely parallel with the spins. Depending on the direction of the sweep, this loads atoms into either the upper or the lower dressed band. We interrupt the sweep at various times, and image the spin-momentum distribution. This reveals that the spin texture follows the effective Zeeman field. We verify that the process is reversible by sweeping the detuning back to δ_i and observing that full spin-polarization is restored, as shown in Fig. 1(f) and 1(g).

Having demonstrated the ability to engineer spin-orbit coupling in a Fermi gas, we introduce a general

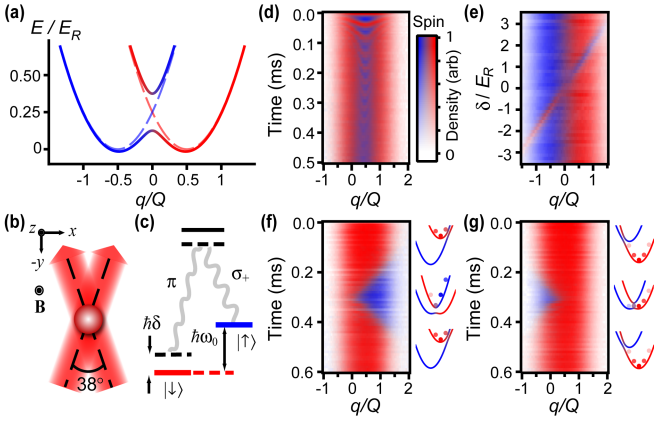

FIG. 1. Realization of spin-orbit coupling in an atomic Fermi gas. (a) Energy bands as a function of quasi-momentum q for Raman coupling strength of $\hbar\Omega_R = 0.25E_R$ and $\hbar\delta = 0E_R$. Energy bands for $\hbar\Omega_R = \hbar\delta = 0E_R$ are shown with dashed lines. Color indicates spin composition of the states. (b) A pair of Raman beams at $\pm 19^\circ$ relative to the $\hat{y}$ axis couples states $|\downarrow, k_x = q\rangle$ and $|\uparrow, k_x = q + Q\rangle$. A bias magnetic field $\mathbf{B}$ in the $\hat{z}$ direction provides the quantization axis. (c) Energy level diagram of states coupled by the Raman fields: $\hbar\delta$ is the two-photon detuning. The hyperfine interaction splits $|\uparrow\rangle$ and $|\downarrow\rangle$ by $\hbar\omega_0$, and the relevant polarization components are π and σ_+. (d) Momentum-dependent Rabi oscillations for $\hbar\Omega_R = 0.71(2)E_R$ and $\hbar\delta = -0.25(1)E_R$. Atoms are prepared in $|\downarrow\rangle$ (red), and are subsequently projected into a superposition of eigenstates as the Raman field is pulsed on. (e) A π-pulse for the resonant momentum class is applied at different $\hbar\delta$ for $\hbar\Omega_R = 0.035(5)E_R$. (f,g): Adiabatic loading and unloading of atoms into the upper (lower) band with $\hbar\Omega_R = 0.53(5)E_R$. The Raman beams are turned on with $\delta = \mp 8.5\Omega_R$, which is then swept linearly to $\delta = 0$ and back at a rate of $|\dot{\delta}| = 0.27(5)\Omega_R^2$.

approach to measure the eigenstates and energies of fermions at each quasi-momentum q and thus resolve the band structure and the spin texture of spin-orbit coupled atomic systems. Our approach yields similar information to spin and angle-resolved photoemission spectroscopy (spin-ARPES), a powerful technique recently developed in condensed matter physics [16]. Spin-ARPES is particularly useful for studying magnetic and quantum spin Hall materials; it has been used, for example, to directly measure topological quantum numbers in the $Bi_{1-x}Sb_x$ series, revealing the presence of topological order and chiral properties [17].

Our spectroscopic technique uses radiofrequency (RF) spin-injection of atoms from a free Fermi gas into an empty spin-orbit coupled system using photons of a known energy, as shown in Fig. 2(a). After injection, the momentum and spin of the injected atoms are analyzed using time of flight [18] combined with spin-resolved detection. Atoms are initially loaded into one of two free "reservoir" atomic states $|\downarrow\rangle_R$ and $|\uparrow\rangle_R$, for which we use the first and fourth lowest hyperfine states of ^{6}Li.

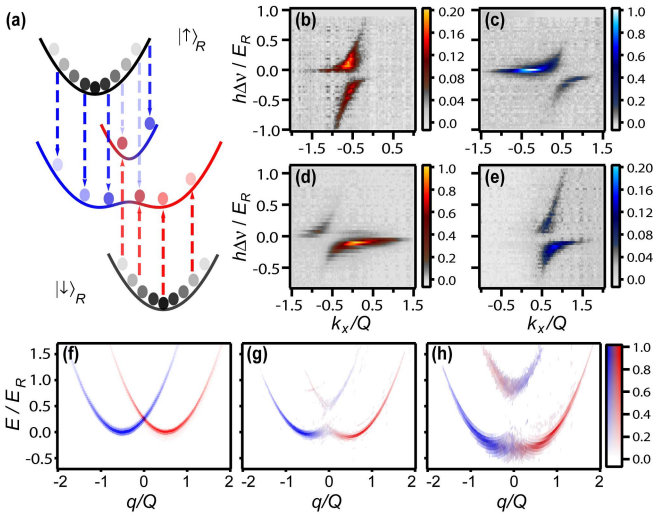

FIG. 2. Spin-injection spectroscopy. (a) An RF pulse injects atoms from the reservoir states (shown in black) $|\uparrow\rangle_R$ and $|\downarrow\rangle_R$ into the spin-orbit coupled system (shown in red and blue). Injection occurs when the RF photon energy equals the energy difference between the reservoir state and the spin-orbit coupled state at quasi-momentum q. (b,c) Spin-resolved $|\downarrow\rangle$ and $|\uparrow\rangle$ spectra, respectively, when transferring out of $|\uparrow\rangle_R$. Here, $\hbar\Omega_R = 0.43(5)E_R$ and $\hbar\delta = 0.00(3)E_R$. (d,e) Spin-resolved $|\downarrow\rangle$ and $|\uparrow\rangle$ spectra, respectively, when transferring out of $|\downarrow\rangle_R$ for the same Raman strength $\hbar\Omega_R$. (f, g and h) The reconstructed spinful dispersions for $\hbar\delta = 0.00(3)E_R$ and $\hbar\Omega_R = 0E_R$, $\hbar\Omega_R = 0.43(5)E_R$ and $\hbar\Omega_R = 0.9(1)E_R$, respectively.

State $|\downarrow\rangle_R$ can be coupled via RF to the state $|\downarrow\rangle$, as this connects the first and second lowest hyperfine states. Similarly, an atom in state $|\uparrow\rangle_R$ can be transferred to $|\uparrow\rangle$. RF spin-injection does not impart momentum to the atom, and occurs when the frequency of the RF pulse matches the energy difference between the spin-orbit coupled bands and the initial reservoir state, as shown in Fig. 2(a). Spin-injection from $|\downarrow\rangle_R$ ($|\uparrow\rangle_R$) populates mostly the region of the spin-orbit coupled bands with a strong admixture of $|\downarrow\rangle$ ($|\uparrow\rangle$) states. Thus, the use of two reservoir states allows us to measure both the $|\downarrow\rangle$-rich and the $|\uparrow\rangle$-rich parts of the spin-orbit coupled bands. Following the injection process, the Raman beams are switched off, and the atoms are simultaneously released from the trap. By counting the number of atoms of a given spin and momentum as a function of injection energy after time-of-flight, we determine the dispersion of the spin-orbit coupled bands along with their spin texture. Note that while spin-ARPES and previous momentum-resolved spectroscopic techniques in ultracold atoms probe the occupied states of a given system, our spin-injection method probes the unoccupied states. In the case of fermionic superfluids, this would reveal the excited branch of the quasi-particle dispersion.

The topological characteristics of the bands, which are encoded in the eigenstates, can be extracted from the spin and momentum composition. For our spin-orbit system with $\delta = 0$, the spin of the eigenstates is confined to the y-z plane on the Bloch sphere because the effective magnetic field has no $\hat{x}$ component. More general couplings may not restrict the spin to a great circle on the Bloch sphere, in which case at least two spin components must be measured for a complete characterization of the bands. This can be achieved by rotating the different spin components onto the measurement basis with an RF pulse.

Applying spin-injection spectroscopy, we have measured the band structure of the equal-part Rashba-Dresselhaus Hamiltonian at $\delta = 0$ for several Ω_R. Figures 2(b), 2(c), 2(d) and 2(e) show spin- and momentum-resolved spin-injection spectra obtained with atoms starting in the $|\uparrow\rangle_R$ reservoir (top row) and starting in the $|\downarrow\rangle_R$ reservoir (bottom row), for the case $\hbar\Omega_R = 0.43(5)E_R$ and $\delta = 0$. The $(q,\uparrow) \leftrightarrow (-q,\downarrow)$ symmetry of the system can be seen in the spectra in Fig. 2. The energy at each quasimomentum is found by adding the energy injected into the system by the RF pulse to the initial kinetic energy of the free particle in the reservoir. Figures 2(f), 2(g) and 2(h) show the dispersion and spin texture of the bands obtained from the data. As Ω_R is increased, we observe the opening of a spin-orbit gap at $q = 0$. The spin composition of the bands evolves from purely $|\uparrow\rangle$ or $|\downarrow\rangle$ away from the spin-orbit gap to a mixture of the two spin states in the vicinity of the spin-orbit gap, where the spin states are resonantly coupled.

A Fermi gas with the above dispersion has a spinful semi-metallic behavior when the Fermi energy lies within the spin-orbit gap. When the Fermi energy is outside the spin-orbit gap, there is a four-fold degeneracy of states at the Fermi surface. Inside the gap, however, the degeneracy is halved. Furthermore, propagation of spin up particles at the Fermi energy can only occur in the positive q direction, while spin down fermions can only propagate in the opposite direction. For energies within the gap, the system thus acts as a spin-current diode.

An even richer band structure involving multiple spinful bands separated by fully insulating gaps can arise in the presence of a periodic lattice potential. This has been realized for Bose-Einstein condensates by adding RF coupling between the Raman-coupled states $|\uparrow\rangle$ and $|\downarrow\rangle$ [19]. Using a similar method, we create a spinful lattice for ultracold fermions, and use spin-injection spectroscopy to probe the resulting spinful band structure. The combined Raman/RF coupling scheme is shown in Fig. 3(a). The Raman field couples the states $|\downarrow, k_x = q\rangle$ and $|\uparrow, k_x = q + Q\rangle$ with strength Ω_R, whereas the RF field couples the states $|\downarrow, k_x = q\rangle$ and $|\uparrow, k_x = q\rangle$ with strength Ω_{RF}. As a result, the set of coupled states for a given quasimomentum q, shown in the repeated Brillouin scheme in Fig. 3(b), is $|\sigma, k_x = q + nQ\rangle$ for integer n and $\sigma = \uparrow, \downarrow$. The lowest four bands are degenerate at

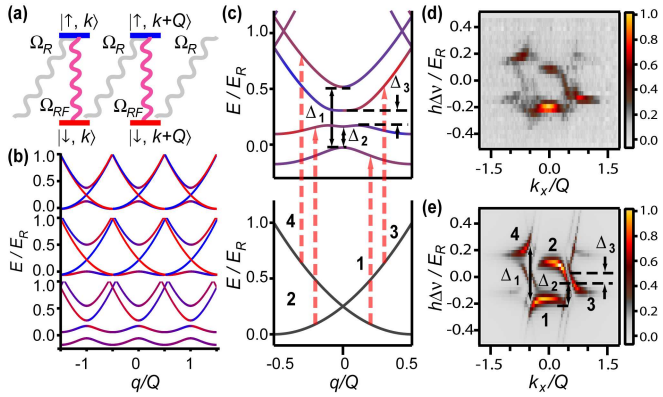

FIG. 3. Creating and probing a spin-orbit coupled lattice. (a) The addition of a radiofrequency field allows momentum transfer of any multiple of Q, producing a spinful lattice band structure. (b) The band structure of the Raman-RF system in the repeated zone scheme. Bandstructures from top to bottom correspond to: $\hbar\Omega_{RF} = 0$ and $\hbar\Omega_R = 0.25E_R$, $\hbar\Omega_R = 0.5E_R$ and $\hbar\Omega_{RF} = 0$, and $\hbar\Omega_R = 0.5E_R$ and $\hbar\Omega_{RF} = 0.25E_R$. In the bottommost band, all degeneracies are lifted. (c) Spin injection from free particle bands to spinful lattice bands, starting from $|\downarrow\rangle_R$. Transitions near zero RF detuning ($h\Delta\nu \sim 0$) that give rise to dominant spectral features are identified. (d) Experimental spectrum of the Raman-RF system with $\hbar\Omega_R = 0.40(5)E_R$ and $\hbar\Omega_{RF} = 0.28(2)E_R$ in the spin $|\downarrow\rangle$ channel after injection from reservoir $|\downarrow\rangle_R$. (e) The theoretical spectra corresponding to Fig. 3(d). Features corresponding to the gaps and transitions identified in Fig. 3(c) are labeled.

the band center $q = 0$ when $\Omega_R = \Omega_{RF} = 0$. The Raman field splits the degeneracy between the first and fourth band, leaving the other two degenerate. The remaining degeneracy, which is a Dirac point, is removed with the addition of the RF field. Thus, when the system is filled up to the top of the second band, it is an insulator. Furthermore, when Ω_{RF} is large enough, a band gap also opens between the first and second bands.

Fig. 3(d) shows the $|\downarrow\rangle$ channel of the spin-injection spectra, measured with fermions initially in reservoir state $|\downarrow\rangle_R$. Spectra with injection from $|\downarrow\rangle_R$ is sufficient to reconstruct the full band structure given the $(q, \uparrow) \leftrightarrow (-q, \downarrow)$ symmetry of the Hamiltonian. The transitions between the reservoir and the spin-orbit coupled bands for $\hbar\Omega_R = 0.40(5)E_R$ and $\hbar\Omega_{RF} = 0.28(2)E_R$ are shown in Fig. 3(c). The experimental spectrum in Fig. 3d is compared to the theoretically calculated spectrum, shown in Fig. 3(e). The spectrum exhibits four prominent features separated by three energy gaps, labeled Δ_1, Δ_2 and Δ_3 in Fig. 3(e). The gaps giving rise to these features are shown on the band structure in Fig. 3(c). The gap Δ_1 is opened by the spin-orbit coupling, while Δ_2 is opened by a direct RF coupling and Δ_3 is opened by a second order process that involves both the RF and Raman fields, explaining its smallness. We have explored the Raman/RF system for a range of coupling strengths as shown in the spectra in Fig. 4(a) and 4(b). With a careful choice of the Raman/RF coupling strengths, spinful flat bands can be realized (see Supplemental Material Fig. S3), where interactions should play a dominant role [20].

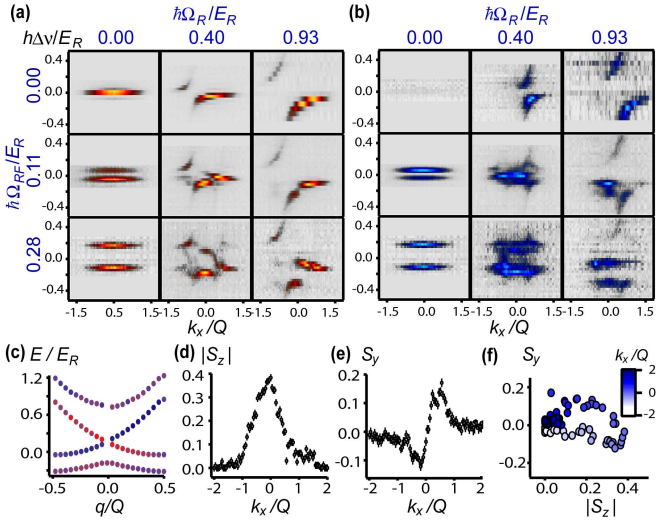

FIG. 4. Evolution of spin-textured energy bands of a spin-orbit coupled lattice. (a,b) Experimental Raman-RF spin-injection spectra for injection from $|\downarrow\rangle_R$ for channels $|\downarrow\rangle$ and $|\uparrow\rangle$, respectively. The color map used is the same as Fig. 2(b) and 2(e) after rescaling to the maximum intensity. Interaction effects between $|\uparrow\rangle$ with $|\downarrow\rangle_R$ (see Fig. S4) makes only the dominant features resolvable in $|\uparrow\rangle$, while finer features are visible in $|\downarrow\rangle$. (c) Reconstructed band structure for $\hbar\Omega_R = 0.93(7)E_R$ and $\hbar\Omega_{RF} = 0.28(2)E_R$. Color indicates the spin texture. (d,e,f) Experimentally measured spin components S_y and $|S_z|$ as a function of momentum k_x for the lattice wavefunctions corresponding to the bottommost band in Fig. 4(c).

To illustrate how the energy bands along with the corresponding eigenstates can be extracted, we reconstruct the energy bands along with the spin texture for $\hbar\Omega_R = 0.93(7)E_R$ and $\hbar\Omega_{RF} = 0.28(2)E_R$, as shown in Fig. 4(c). The energies of the bands are obtained from the resonant frequencies in the spin-injection spectra, while the spin composition $S_{y,z}$ is extracted from the relative weights of the signal in the two spin channels (see Supplemental Material). In Fig. 4(d), 4(e) and 4(f), we show the extracted value of $S_y(k_x)$ and $|S_z(k_x)|$ for the bottommost band when $\hbar\Omega_R = 0.93(7)E_R$ and $\hbar\Omega_{RF} = 0.28(2)E_R$. For more general spin-orbit Hamiltonians involving σ_x, one can extract the phase between all three components of $\vec{S}(k_x)$ with additional RF pulses, and fully characterize the eigenstate for the corresponding quasimomentum q. The topology of the band, encoded in the evolution of its eigenstates across the Brillouin zone, can thus be measured.

In summary, we have created and directly probed a spin-orbit gap in a Fermi gas of ultracold atoms and realized a fully gapped band structure allowing for spinful

flat bands. We introduced spin-injection spectroscopy to characterize the spin-textured energy-momentum dispersion. We further show that spin-injection spectroscopy allows reconstruction of eigenstates in a spinful lattice system. Extensions of this method can reveal the nontrivial topology of bands in more general spin-orbit coupled systems [21], opening a path to probing topological insulators with ultracold atoms. Similar spectroscopic techniques should allow the demonstration of effective p-wave interactions in a single component spin-orbit coupled Fermi gas, either near an s-wave Feshbach resonance, or for flat bands as realized here. In these systems, interactions may lead to BCS pairing in a p-wave channel, and in a two-dimensional Fermi gas with pure Rashba coupling, to $p_x + ip_y$ pairing and chiral superfluidity [22, 23].

This work was supported by the NSF, a grant from the Army Research Office with funding from the DARPA OLE program, ARO-MURI on Atomtronics, AFOSR-MURI, ONR YIP, DARPA YFA, an AFOSR PECASE, and the David and Lucile Packard Foundation. Z. H. acknowledges funding from EPSRC under Grant No. EP/I010580/1.

[1] M. Z. Hasan and C. L. Kane, Rev. Mod. Phys. **82**, 3045 (2010).
[2] X.-L. Qi and S.-C. Zhang, Rev. Mod. Phys. **83**, 1057 (2011).
[3] R. Winkler, *Spin-Orbit Coupling Effects in Two-Dimensional Electron and Hole Systems*, Springer Tracts in Modern Physics, Vol. 191 (Springer, Berlin, 2003).
[4] Y. A. Bychkov and E. I. Rashba, J. Phys. C **17**, 6039 (1984).
[5] G. Dresselhaus, Phys. Rev. **100**, 580 (1955).
[6] C. H. L. Quay, T. L. Hughes, J. A. Sulpizio, L. N. Pfeiffer, K. W. Baldwin, K. W. West, D. Goldhaber-Gordon, and R. de Picciotto, Nat. Phys. **6**, 336 (2010).
[7] S. Nadj-Perge, V. S. Pribiag, J. W. G. van den Berg, K. Zuo, S. R. Plissard, E. P. A. M. Bakkers, S. M. Frolov, and L. P. Kouwenhoven, Phys. Rev. Lett. **108**, 166801 (2012).
[8] X.-J. Liu, M. F. Borunda, X. Liu, and J. Sinova, Phys. Rev. Lett. **102**, 046402 (2009).
[9] J. Dalibard, F. Gerbier, G. Juzeliūnas, and P. Öhberg, Rev. Mod. Phys. **83**, 1523 (2011).
[10] Y.-J. Lin, Jiménez-García, and I. B. Spielman, Nature **471**, 83 (2011).
[11] Y.-J. Lin, R. L. Compton, Jiménez-García, J. V. Porto, and I. B. Spielman, Nature **462**, 628 (2009).
[12] M. Aidelsburger, M. Atala, S. Nascimbène, S. Trotzky, Y.-A. Chen, and I. Bloch, Phys. Rev. Lett. **107**, 255301 (2011).
[13] P. Wang, Z.-Q. Yu, Z. Fu, J. Miao, L. Huang, S. Chai, H. Zhai, and J. Zhang, arXiv:1204.1887v1 [cond-mat.quant-gas] (2012).
[14] E. Zhao, N. Bray-Ali, C. J. Williams, I. B. Spielman, and I. I. Satija, Phys. Rev. A **84**, 063629 (2011).
[15] Z. Hadzibabic, S. Gupta, C. A. Stan, C. H. Schunck, M. W. Zwierlein, K. Dieckmann, and W. Ketterle, Phys. Rev. Lett. **91**, 160401 (2003).
[16] M. Hoesch, T. Greber, V. N. Petrov, M. Muntwiler, M. Hengsberger, W. Auwrter, and J. Osterwalder, Journal of Electron Spectroscopy and Related Phenomena **124**, 263 (2002).
[17] D. Hsieh, Y. Xia, L. Wray, D. Qian, A. Pal, J. H. Dil, J. Osterwalder, F. Meier, G. Bihlmayer, C. L. Kane, Y. S. Hor, R. J. Cava, and M. Z. Hasan, Science **323**, 919 (2009).
[18] J. T. Stewart, J. P. Gaebler, and D. S. Jin, Nature **454**, 744 (2008).
[19] K. Jiménez-García, L. J. LeBlanc, R. A. Williams, M. C. Beeler, A. R. Perry, and I. B. Spielman, Phys. Rev. Lett. **108**, 225303 (2012).
[20] K. Sun, Z. Gu, H. Katsura, and S. Das Sarma, Phys. Rev. Lett. **106**, 236803 (2011).
[21] J. D. Sau, R. Sensarma, S. Powell, I. B. Spielman, and S. Das Sarma, Phys. Rev. B **83**, 140510 (2011).
[22] R. A. Williams, L. J. LeBlanc, K. Jiménez-García, M. C. Beeler, A. R. Perry, W. D. Phillips, and I. B. Spielman, Science **335**, 314 (2012).
[23] C. Zhang, S. Tewari, R. M. Lutchyn, and S. Das Sarma, Phys. Rev. Lett. **101**, 160401 (2008).